Robotica: (2020) volume 38, pp. 1400–1414. © Cambridge University Press 2019
doi:10.1017/S026357471900153X

Energy-Optimal Motion Trajectory of an Omni-Directional Mecanum-Wheeled Robot via Polynomial Functions

Li Xie*, Karl Stol and Weiliang Xu

Department of Mechanical Engineering, University of Auckland (UoA), Auckland, New Zealand
E-mails: k.stol@auckland.ac.nz, p.xu@auckland.ac.nz

(Accepted October 9, 2019. First published online: November 6, 2019)

SUMMARY
The Mecanum wheel is one of the practical omni-directional wheel designs in industry, especially for heavy-duty tasks in a confined floor. An issue with Mecanum-wheeled robots is inefficient use of energy. In this study, the robotic motion trajectories are optimized to minimize the energy consumption, where a robotic path is expressed in polynomial functions passing through a given set of via points, and a genetic algorithm is used to find the polynomial's coefficients being decision variables. To attempt a further reduction in the energy consumption, the via points are also taken as decision variables for the optimization. Both simulations and experiments are conducted, and the results show that the optimized trajectories result in a significant reduction in energy consumption, which can be further lowered when the via points become decision variables. It is also found that the higher the order of the polynomials the larger the reduction in the energy consumption.

KEYWORDS: Mecanum wheel; Omni-directional robot; Energy optimization; Motion planning; Trajectory generation.

1. Introduction

Omni-directional mobile robots can transport materials without difficulty in congested, confined, and highly dynamic environments. The Ilon Mecanum wheel is a practical omni-directional drive solution in industry.[1] The Mecanum wheel has an advantage of high-load capacity over other omni-directional wheel designs.[2] However, the Mecanum drive is inefficient in use of energy when the robot does not move in a straight line, which is especially critical in heavy-duty industrial applications.[3] The Mecanum robot is holonomic and can reach the same goal pose via various feasible motion trajectories, which consume a varying amount of energy. Thus, planning the energy-optimal motion trajectories for the Mecanum robot is a valid strategy to reduce its energy consumption, which has been explored very little yet.

Mei et al.[4] proposed a motion planning method to reduce the energy consumption of mobile robots and showed that by utilizing different path plans and velocity schedules, the robot achieved up to 51% energy savings for a same task. Sun and Reif[5] proposed a minimum-energy path planning method for mobile robots on different terrains where the energy consumption was related only to the gravitational force and friction. Liu and Sun[6] put forward an energy model for a wheeled mobile robot and added a new energy-related criterion into the A* algorithm for the purpose of searching for the minimum-energy path where a parameterized trajectory in the cubic Bezier curve was employed. Yang et al.[7] applied polynomial parameterization to plan a real-time and near minimum-energy path for carlike mobile robots, while Duleba and Sasiadek[8] modified the Newton algorithm to optimize the energy consumption in the nonholonomic motion planning. The minimum-energy trajectory planning

* Corresponding author. E-mail: lxie021@aucklanduni.ac.nz

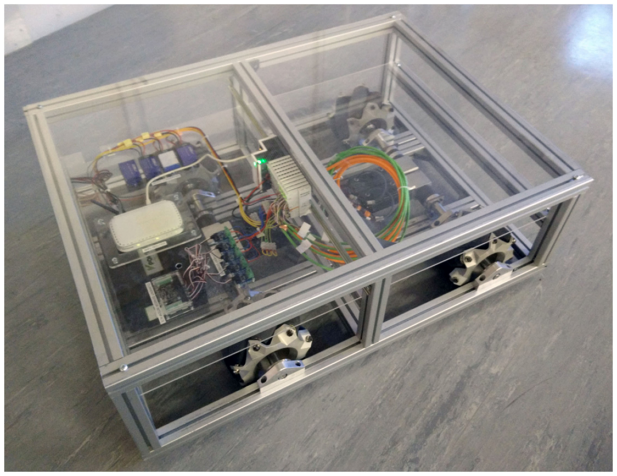

Fig. 1. The Mecanum robot.

method by Kim and Kim[9,10] is for both nonholonomic and holonomic robots, where the velocity profiles are found online.

The polynomial-based trajectory has been common to mobile robotics and manipulative robotics. Paul and Zhang[11] were the first to utilize polynomials for robotic trajectory generation. Shintaku[12] utilized a polynomial to approximate the joint-space trajectories of an underwater manipulator and applied a genetic algorithm (GA) to search for the optimal polynomial coefficients that minimize the energy consumption. Tian and Collins[13] planned the task-space trajectories of a robotic manipulator utilizing the Hermite cubic polynomial and then applied a GA for finding the optimal polynomial coefficients. Yang et al.[14] proposed a path planning method for mobile robots, which utilizes the Bezier curve and optimizes the Bezier control points for the minimal time.

In this paper, an offline energy-optimal trajectory planning problem for the Mecanum-wheeled robots in a static environment is formulated and studied. Given a sequence of via points of a path, including stationary initial and goal poses, the energy-optimal motion trajectories are generated, subjected to the constraints of continuous velocities and accelerations at the via points. The trajectories are expressed in polynomial functions of time for both translational and rotational degrees of motion, and both the coefficients of the polynomials and the via points are optimized by GA via an energy consumption model developed in ref. [15].

Compared to the existing works in the literature, this paper has the following highlights. First, this paper solves a practical issue with industrial Mecanum robots by applying an established method. High-energy consumption is a weakness to the heavy-duty Mecanum robots. Applying the polynomial-based trajectory generation to the Mecanum robots (that are holonomic) for energy optimization has not been studied yet. Second, both the coefficients of the polynomials and the via points for path can be optimized simultaneously, which gives rise to the greater reduction in energy consumption for a given motion task. Third, the total energy consumed by all onboard facilities such as controllers, motor drives, sensors, and chassis of the robot is considered as the cost function for optimization.

2. Mecanum Robot and Its Energy Consumption

2.1. Mecanum robot

An image of the robot used in this study is shown in Fig. 1, with the system parameters given in Table I.

The schematic diagram of the robot is depicted in Fig. 2, where Ox_ry_r is the robotic coordinate system, rigidly attached at the mass center of the chassis and OX_GY_G is the global coordinate system. Angle $\emptyset$ is the angular displacement or orientation of the robot, and translational displacements X and Y define the center of mass of the robot. The pose of the robot is represented by $\boldsymbol{q} = [X\ Y\ \emptyset]^T$ in OX_GY_G.

https://doi.org/10.1017/S026357471900153X Published online by Cambridge University Press

Table I. Model parameters of the robot.

Symbol	Quantity	Value
r	Wheel radius	0.11 m
l_x	Distance from the center of robot to the center of Mecanum wheel in x directions	0.45 m
l_y	Distance from the center of robot to the center of Mecanum wheel in x directions	0.60 m
m	Mass of robot	94.00 kg
I	Moment of inertia of robot in the z direction	19.40 kg · m^2
J_w	Moment of inertia of the Mecanum wheel along its rotation axis	0.04 kg · m^2
P_{idle}	Idling robotic power consumption	72.00 W
$\dot{X}_{max}$	Maximum velocity in translation X	0.10 m/s
$\dot{Y}_{max}$	Maximum velocity in translation Y	0.10 m/s
$\dot{\emptyset}_{max}$	Maximum velocity in translation $\emptyset$	0.10 rad/s
$\ddot{X}_{max}$	Maximum acceleration in translation X	0.50 m/s^2
$\ddot{Y}_{max}$	Maximum acceleration in translation Y	0.50 m/s^2
$\ddot{\emptyset}_{max}$	Maximum acceleration in translation $\emptyset$	0.50 rad/s^2

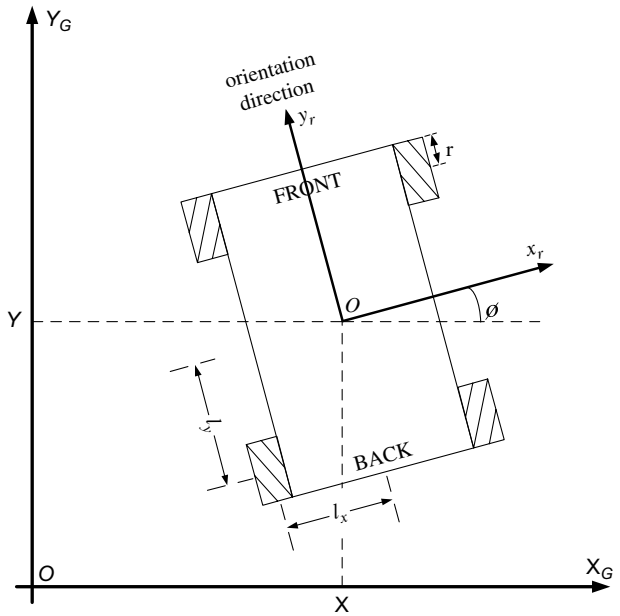

Fig. 2. Schematic diagram of the robot.

2.2. *Energy consumption model*

The energy consumption model of the robot was developed in refs. [15, 16]. The total energy consumption of the robot E_{total} is expressed by

$$E_{total} = E_{idle} + E_{motion} \tag{1}$$

where $E_{idle} = \int_t P_{idle}\, dt$ is the idle energy consumed by the idling robot consisting of the idling motors and onboard electric devices; $E_{motion} = \int_t P_{motion}\, dt = E_k + E_f + E_e + E_m$ is the motional energy consumed to attain and sustain robotic motion. Here, E_k, E_f, E_e, and E_m are, respectively, the changes in robot kinetic energy, the frictional dissipation to overcome the traction resistances, the energy dissipation as heat in the armatures of motors, and the mechanical dissipation caused by overcoming the friction torque in the motors including motor shafts and bearings.

https://doi.org/10.1017/S026357471900153X Published online by Cambridge University Press

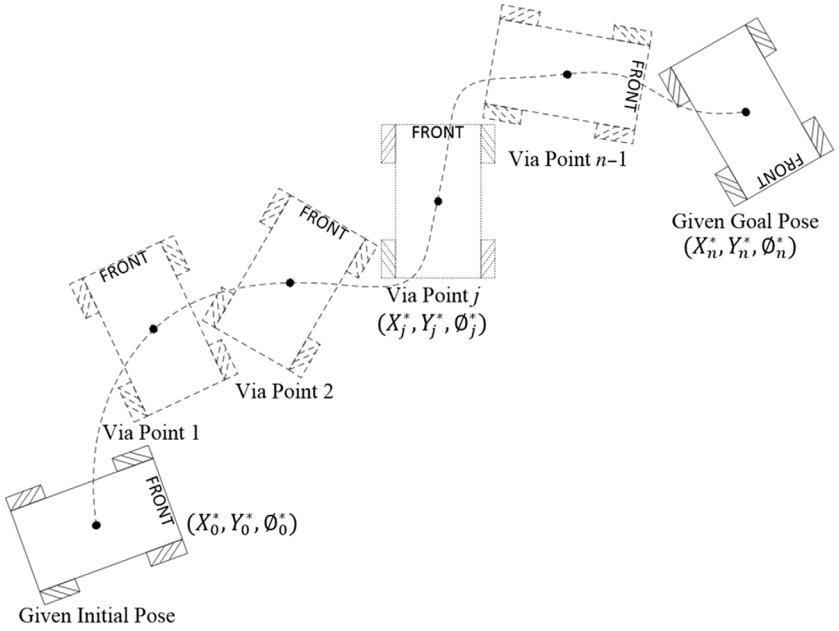

Fig. 3. Path points in task space including initial pose, via points, and goal pose.

3. Energy-Optimal Trajectory Generation

3.1. Trajectories of the omni-directional Mecanum robot in polynomial functions

The trajectories of the omni-directional Mecanum robots consist of the nine time functions of the position, velocity, and acceleration in three degrees of freedom that are translation X, translation Y, and rotation $\emptyset$. The polynomial spline function is chosen to express the task-space trajectories. Given a path including an initial pose $(X_0^*, Y_0^*, \emptyset_0^*)$ and a goal pose $(X_n^*, Y_n^*, \emptyset_n^*)$ with or without a sequence of via points $(X_1^*, Y_1^*, \emptyset_1^*), \ldots, (X_{n-1}^*, Y_{n-1}^*, \emptyset_{n-1}^*)$ in the task space, the robot must reach these path points at time $t_0, t_1, \ldots, t_n$, respectively. Time t_n is also named as task duration. Here, $(X_j^*, Y_j^*, \emptyset_j^*)$ is the jth via point for $j = 1, 2, 3, \ldots, n-1$ as shown in Fig. 3.

The desired pose matrices are defined as follows,

$$\boldsymbol{X} = \left[X_0^* \; X_1^* \; X_2^* \; \ldots \; X_j^* \; \ldots \; X_n^*\right]^T \tag{2}$$

$$\boldsymbol{Y} = \left[Y_0^* \; Y_1^* \; Y_2^* \; \ldots \; Y_j^* \; \ldots \; Y_n^*\right]^T \tag{3}$$

$$\boldsymbol{\Phi} = \left[\emptyset_0^* \; \emptyset_1^* \; \emptyset_2^* \; \ldots \; \emptyset_j^* \; \ldots \; \emptyset_n^*\right]^T \tag{4}$$

To pass through a sequence of $n+1$ path points, a set of three time functions of n segments of k-order splines is utilized to express the X, Y, and $\emptyset$ trajectories.

$$\begin{aligned} X_i(t) = a_{i0} + a_{i1}\,(t - t_{i-1}) + a_{i2}(t - t_{i-1})^2 \\ + \cdots + a_{ik}(t - t_{i-1})^k \end{aligned} \tag{5}$$

$$\begin{aligned} Y_i(t) = b_{i0} + b_{i1}\,(t - t_{i-1}) + b_{i2}(t - t_{i-1})^2 \\ + \cdots + b_{ik}(t - t_{i-1})^k \end{aligned} \tag{6}$$

$$\begin{aligned} \emptyset_i(t) = c_{i0} + c_{i1}\,(t - t_{i-1}) + c_{i2}(t - t_{i-1})^2 \\ + \cdots + c_{ik}(t - t_{i-1})^k \end{aligned} \tag{7}$$

https://doi.org/10.1017/S026357471900153X Published online by Cambridge University Press

where $i = 1, 2, \ldots, n$ determines the ith piecewise trajectory, $a_{i0}, a_{i1}, \ldots, a_{ik}, b_{i0}, b_{i1}, \ldots, b_{ik}, c_{i0}, c_{i1}, \ldots, c_{ik}$ are the parameters of the splines, and $t \in [t_{i-1}, t_i]$ is the time. $X(t)$ is the final time function of the position trajectories that contain all $X_i(t)$. Then $\dot{X}(t)$ and $\ddot{X}(t)$ are denoted as the first and second derivatives of $X(t)$. By analogy, $Y(t)$, $\dot{Y}(t)$, $\ddot{Y}(t)$, $\emptyset(t)$, $\dot{\emptyset}(t)$, and $\ddot{\emptyset}(t)$ are defined. The rest of this section covers only the trajectories in translation X.

To find the feasible trajectories that satisfy the requirements, the following three basic conditions A, B, and C must be met.

A. The trajectories must pass through the given path points at the corresponding time

$$X_i(t_{i-1}) = X^*_{i-1}, \; X_i(t_i) = X^*_i \tag{8}$$

B. The trajectories are velocity continuous at via points

$$\dot{X}_i(t_i) = \dot{X}_{i+1}(t_i) \tag{9}$$

C. The trajectories are acceleration continuous at via points

$$\ddot{X}_i(t_i) = \ddot{X}_{i+1}(t_i) \tag{10}$$

The above conditions can be mathematically represented by

$$a_{i0} = X^*_{i-1} \tag{11}$$

$$a_{i0} + a_{i1}\Delta t_i + a_{i2}\Delta t_i^2 + \cdots + a_{ik}\Delta t_i^k = X^*_i \tag{12}$$

$$a_{i1} + 2a_{i2}\Delta t_i + \cdots + k a_{ik}\Delta t_i^{k-1} = a_{(i+1)1} \tag{13}$$

$$2a_{i2} + 6a_{i3}\Delta t_i + \cdots + k(k-1)\, a_{ik}\Delta t_i^{k-2} = 2a_{(i+1)2} \tag{14}$$

in which $\Delta t_i = t_i - t_{i-1}$ are the spline time variables. The spline time variable matrix $\boldsymbol{\Delta t}$ is defined as $[\Delta t_1 \; \Delta t_2 \ldots \; \Delta t_n]^T$. The spline parameter matrix $\boldsymbol{a_0}$ is defined as $[a_{10} \; a_{20} \ldots \; a_{n0}]^T$, and $\boldsymbol{a_1}, \boldsymbol{a_2}, \ldots, \boldsymbol{a_k}$ are defined in a similar way. A partial set of the spline parameters is determined by the conditions A, B, and C. The rest of the undetermined spline parameters are treated as decision variables in this study.

Basic condition A:

$$\boldsymbol{a_0} = \boldsymbol{X} \tag{15}$$

Basic conditions A and B:

$$a_{i2} = \frac{3\left(X^*_i - X^*_{i-1}\right)}{\Delta t_i^2} - \frac{2a_{i1} + a_{(i+1)1}}{\Delta t_i} + a_{i4}\Delta t_i^2 + 2a_{i5}\Delta t_i^3 + \cdots + (k-3)\, a_{ik}\Delta t_i^{k-2} \tag{16}$$

$$a_{i3} = \frac{2\left(X^*_{i-1} - X^*_i\right)}{\Delta t_i^3} + \frac{a_{i1} + a_{(i+1)1}}{\Delta t_i^2} - 2a_{i4}\Delta t_i - 3a_{i5}\Delta t_i^2 - \cdots - (k-2)\, a_{ik}\Delta t_i^{k-3} \tag{17}$$

Basic condition C:

$$\frac{2a_{i1} + 4a_{(i+1)1}}{\Delta t_i} + \frac{4a_{(i+1)1} + 2a_{(i+2)1}}{\Delta t_{i+1}} = \frac{6\left(X^*_i - X^*_{i-1}\right)}{\Delta t_i^2} + \frac{6\left(X^*_{i+1} - X^*_i\right)}{\Delta t_{i+1}^2} - 2a_{i4}\Delta t_i^2 - 6a_{i5}\Delta t_i^3 - \cdots - \left(k^2 - 5k + 6\right) a_{ik}\Delta t_i^{k-2} + 2a_{(i+1)4}\Delta t_{i+1}^2 + 4a_{(i+1)5}\Delta t_{i+1}^3 + \cdots + 2(k-3)\, a_{(i+1)k}\Delta t_{i+1}^{k-2} \tag{18}$$

To satisfy the given conditions, the spline functions require a minimum order of 3.

https://doi.org/10.1017/S026357471900153X Published online by Cambridge University Press

3.2. Parameter optimization

To find the energy-optimal trajectories for the Mecanum robot, a set of decision variables is chosen, which are spline time variables $\Delta \boldsymbol{t}$, spline parameters $\boldsymbol{a_4}, \boldsymbol{b_4}, \boldsymbol{c_4}, \boldsymbol{a_5}, \boldsymbol{b_5}, \boldsymbol{c_5}, \ldots, \boldsymbol{a_k}, \boldsymbol{b_k}, \boldsymbol{c_k}$, and optionally via points $(X_1^*, Y_1^*, \emptyset_1^*), \ldots, (X_{n-1}^*, Y_{n-1}^*, \emptyset_{n-1}^*)$. The total number of decision variables N_{dv} depends on the number and order of the splines, and the number of the optional via points. Via points can be optional and once chosen, they are called the relaxed via points in this paper, denoted as N_{rvp},

$$N_{\text{dv}} = n + 3 * n * (k-3) + 3 * N_{\text{rvp}} \tag{19}$$

As each piecewise trajectory has one spline time variable as the decision variable, the total number of the spline time variables is the same as the number of the piecewise trajectories n. The undetermined spline parameters are from the fourth-order and higher-order terms. So, the number of the undetermined spline parameters of each piecewise trajectory for each degree of freedom is $k-3$. Every relaxed via point that has three degrees of freedom contributes to three decision variables.

Every combination of decision variables $\boldsymbol{\kappa}$ presents the unique candidate trajectories of the robot in a function of $T(\boldsymbol{\kappa})$ by Eqs. (5)–(7). Among all the candidate trajectories, the minimum-energy trajectory can be found by

$$\begin{aligned}\min_{\boldsymbol{\kappa}} E\left(T\left(\boldsymbol{\kappa}\right)\right), \boldsymbol{\kappa} = \big[&\Delta \boldsymbol{t}, \boldsymbol{a_4}, \boldsymbol{b_4}, \boldsymbol{c_4}, \boldsymbol{a_5}, \boldsymbol{b_5}, \boldsymbol{c_5}, \ldots, \boldsymbol{a_k}, \boldsymbol{b_k}, \boldsymbol{c_k}, \left(X_1^*, Y_1^*, \emptyset_1^*\right), \ldots, \\ &\left(X_{n-1}^*, Y_{n-1}^*, \emptyset_{n-1}^*\right)\big]\end{aligned} \tag{20}$$

The objective function $E(T(\boldsymbol{\kappa}))$ is based on the energy consumption model of the robot in Eq. (1). The model takes in the time history of positions, velocities, and accelerations for all three degrees of freedom given by $T(\boldsymbol{\kappa})$ and estimates the amount of energy the robot consumes. A GA is used to optimize decision variables that minimize the energy consumption. The GA solver in the MATLAB Optimization Toolbox was utilized in this study.

4. Simulations and Experiments

Simulations and experiments were conducted to evaluate the proposed energy-optimal motion trajectories, where the maximum translational and rotational velocities of the robot were set at 0.1 m/s and 0.1 rad/s, respectively, and the maximum translational and rotational accelerations were set at 0.5 m/s^2 and 0.5 rad/s^2, respectively.

4.1. Simulations

Three sets of simulations were carried out. The first set of three simulations aimed to investigate the influence of the polynomial spline number between the given path points and the influence of relaxing via points on the optimization. The second set of two simulations aimed to investigate the influence of the spline order. The third set of five simulations aimed to investigate the influence of utilizing both task duration and energy consumption as the objective function on the optimization.

4.1.1. The first set of three simulations. In the first set of three simulations, the initial and goal poses, as shown in Fig. 4, were given as $(x_0^*, y_0^*, \varphi_0^*) = (0, 0, -0.5\pi)$ and $(x_n^*, y_n^*, \varphi_n^*) = (2, 2, -0.2\pi)$, respectively. All the spline parameters were determined, because third-order polynomial functions were utilized to express position trajectories. In the scenario considered for Simulation 1, no via points were used and there were three splines between the initial pose and the goal pose, and one decision variable Δt. Aiming to investigate the influence of increasing the polynomial spline number between the given path points, there were nine splines and three decision variables $[\Delta t_1, \Delta t_2, \Delta t_3]$ in the scenario considered for Simulation 2 by intentionally placing two fixed via points between the initial pose and the goal pose. These via points $[x_1^*, y_1^*, \varphi_1^*, x_2^*, y_2^*, \varphi_2^*]$ were relaxed as additional decision variables in Simulation 3, and there were nine splines and nine decision variables. Below are the optimization formulations for Simulations 1, 2, and 3, respectively,

$$min_{\boldsymbol{\kappa}} E\left(T\left(\boldsymbol{\kappa}\right)\right), \boldsymbol{\kappa} = [\Delta t] \qquad s.t.\ \Delta t > 0 \tag{21}$$

$$\min_{\boldsymbol{\kappa}} E\left(T\left(\boldsymbol{\kappa}\right)\right), \boldsymbol{\kappa} = [\Delta t_1, \Delta t_2, \Delta t_3] \quad s.t.\ [\Delta t_1, \Delta t_2, \Delta t_3] > 0 \tag{22}$$

https://doi.org/10.1017/S026357471900153X Published online by Cambridge University Press

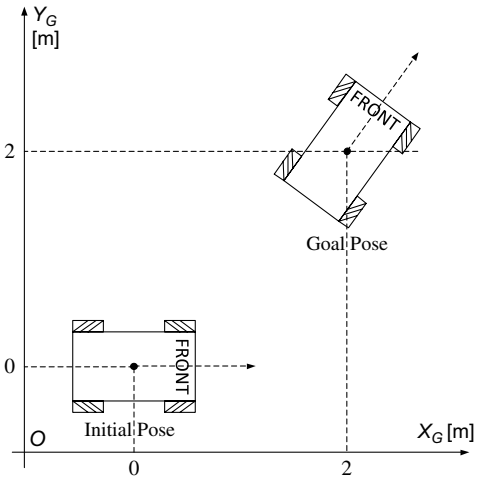

Fig. 4. The initial pose and the goal pose in the first set of simulations.

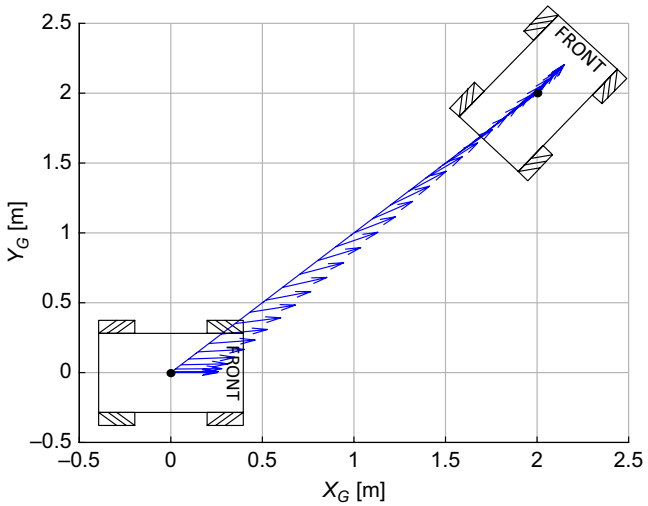

Fig. 5. The energy-optimal trajectories in Simulation 1.

$$\min_{\boldsymbol{\kappa}} E(T(\boldsymbol{\kappa})), \boldsymbol{\kappa} = \left[\Delta t_1, \Delta t_2, \Delta t_3, x_1^*, y_1^*, \varphi_1^*, x_2^*, y_2^*, \varphi_2^*\right] \quad s.t. \ [\Delta t_1, \Delta t_2, \Delta t_3] > 0,$$
$$2 > \left[x_1^*, y_1^*, x_2^*, y_2^*\right] > 0, 0 > \left[\varphi_1^*, \varphi_2^*\right] > -0.7\pi \tag{23}$$

In which the decision variable bounds for time were limited within positive numbers, the decision variable bounds for the relaxed via points were set between the initial pose and the goal pose with extra rotation spaces, as given in Eq. (23).

No via point was used in the scenario considered for Simulation 1 so that $n = 1$. A set of three functions of third-order splines was enough to express the position trajectories of translation X, translation Y, and rotation $\emptyset$. All the spline parameters were determined by the stationary initial pose and the stationary goal pose. Thus, a spline time variable Δt was the only decision variable for energy optimization in Simulation 1. The resultant optimal Δt was 30.1 s, and the resultant optimal energy consumption was 2547.7 J. The resultant energy-optimal trajectories are shown in Fig. 5. In the simulations, the robotic positions are drawn in blue lines and the robotic orientations are represented using blue arrows.

In Simulation 2, two fixed via points were intentionally added with equal distances for translation X, translation Y, and rotation $\emptyset$ and utilized a set of three segments of third-order splines. Two fixed via points were $(x_1^*, y_1^*, \varphi_1^*) = (0.67, 0.67, -0.4\pi)$ and $(x_2^*, y_2^*, \varphi_2^*) = (1.33, 1.33, -0.3\pi)$ so that $n = 3$. The number of the decision variables increases to 3, that is, three spline time variables

https://doi.org/10.1017/S026357471900153X Published online by Cambridge University Press

Table II. Simulation set#1.

Path points	**Optimal decision variables**	**Optimal energy (J)**
Simulation 1		
$(x_0^*, y_0^*, \varphi_0^*) = (0, 0, -0.5\pi)$	$\Delta t = 30.1$ s	
$(x_1^*, y_1^*, \varphi_1^*) = (2, 2, -0.2\pi)$		2547.7
Simulation 2		
$(x_0^*, y_0^*, \varphi_0^*) = (0, 0, -0.5\pi)$	$\Delta \boldsymbol{t} = [9.1\ 8.3\ 9.1]$ s	
$(x_1^*, y_1^*, \varphi_1^*) = (0.67, 0.67, -0.4\pi)$		
$(x_2^*, y_2^*, \varphi_2^*) = (1.33, 1.33, -0.3\pi)$		
$(x_3^*, y_3^*, \varphi_3^*) = (2, 2, -0.2\pi)$		2272.7
Simulation 3		
$(x_0^*, y_0^*, \varphi_0^*) = (0, 0, -0.5\pi)$	$\Delta \boldsymbol{t} = [10\ 10.5\ 5.3]$ s	2200.9
$(x_3^*, y_3^*, \varphi_3^*) = (2, 2, -0.2\pi)$	$(x_1^*, y_1^*, \varphi_1^*) = (0.71, 0.69, 0.06)$	
	$(x_2^*, y_2^*, \varphi_2^*) = (1.66, 1.67, 0.56)$	

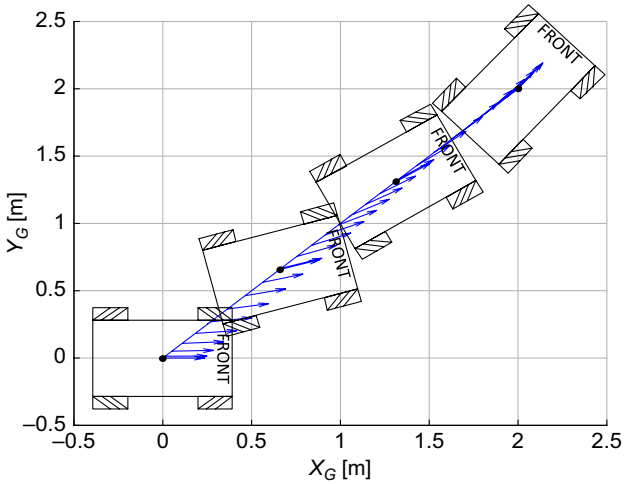

Fig. 6. The energy-optimal trajectories in Simulation 2.

$\Delta \boldsymbol{t}$. The resultant optimal decision variables were found $\Delta \boldsymbol{t} = [9.1\ 8.3\ 9.14]$ s, and the resultant optimal energy consumption was reduced by 10.8% to 2272.7 J. The task duration taken in Simulation 2 was 26.5 s, which is less than 30.1 s for Simulation 1. The resultant energy-optimal trajectories are shown in Fig. 6.

In the scenario considered for Simulation 3, the added via points in Simulation 2 were relaxed as additional decision variables. The locations of the via points and the spline time variables were simultaneously optimized. The decision variable number increases from 3 to 9 by adding $(x_1^*, y_1^*, \varphi_1^*)$ and $(x_2^*, y_2^*, \varphi_2^*)$. The resultant optimal decision variables are given in Table II, and the optimal energy consumption was reduced by an additional 3% to 2200.9 J. The task duration in Simulation 3 was 25.8 s. The resultant energy-optimal trajectories are shown in Fig. 7.

The path points, the optimal decision variables, and the optimal energy consumption in the first set of simulations are given in Table II. The resultant energy-optimal velocity trajectories in Simulations 1–3 are plotted in Fig. 12.

4.1.2. The second set of two simulations. In this set of simulations, the initial pose, the via points, and the goal pose were given as $(x_0^*, y_0^*, \varphi_0^*) = (0, 0, -0.5\pi)$, $(x_1^*, y_1^*, \varphi_1^*) = (2, 1, -0.5\pi)$, $(x_2^*, y_2^*, \varphi_2^*) = (1, 1, -0.5\pi)$, and $(x_3^*, y_3^*, \varphi_3^*) = (2, 2, -0.2\pi)$, as shown in Fig. 8. Both simulations

https://doi.org/10.1017/S026357471900153X Published online by Cambridge University Press

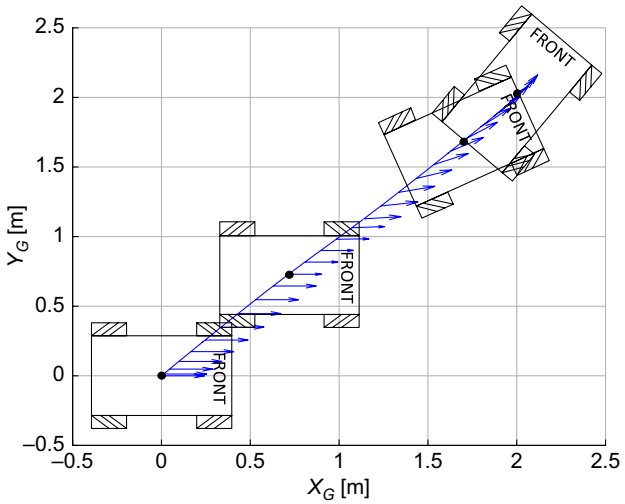

Fig. 7. The energy-optimal trajectories in Simulation 3.

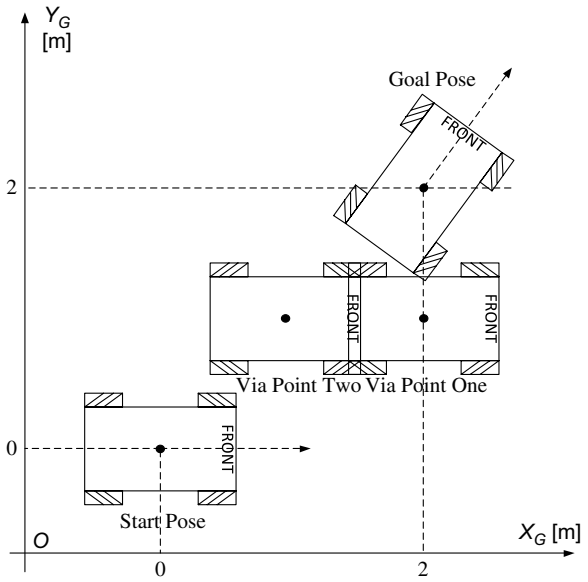

Fig. 8. Path points in the second set of simulations.

used a set of three segments of the splines. In the scenarios considered for Simulations 4 and 5, the third-order and fourth-order splines were used, respectively, for the purpose of investigating the influence of increasing the spline order. There were three decision variables $[\Delta t_1, \Delta t_2, \Delta t_3]$ in Simulation 4, and there were twelve decision variables $[\Delta t_1, \Delta t_2, \Delta t_3, \boldsymbol{a_4}, \boldsymbol{b_4}, \boldsymbol{c_4}]$ in Simulation 5. Below are the optimization formulations for Simulations 4 and 5, respectively,

$$\min_{\boldsymbol{\kappa}} E(T(\boldsymbol{\kappa})), \boldsymbol{\kappa} = [\Delta t_1, \Delta t_2, \Delta t_3] \quad s.t. \ [\Delta t_1, \Delta t_2, \Delta t_3] > 0 \tag{24}$$

$$\min_{\boldsymbol{\kappa}} E(T(\boldsymbol{\kappa})), \boldsymbol{\kappa} = [\Delta t_1, \Delta t_2, \Delta t_3, \boldsymbol{a_4}, \boldsymbol{b_4}, \boldsymbol{c_4}] \quad s.t. \ [\Delta t_1, \Delta t_2, \Delta t_3] > 0 \tag{25}$$

Since the cubic splines were utilized in the scenario considered for Simulation 4, all the spline parameters were determined by the given path points. Two via points were used in the scenario considered for Simulation 4 so that three segments of the trajectories exist between the initial pose and the goal pose. Three spline time variables were the decision variables. The resultant optimal

https://doi.org/10.1017/S026357471900153X Published online by Cambridge University Press

Table III. Simulation set#2.

Optimal decision variables	**Optimal energy (J)**
Simulation 4	
$\Delta \boldsymbol{t} = [31.2\ 21.5\ 13.8]$ s	5497.7
Simulation 5	
$\Delta \boldsymbol{t} = [30.5\ 17.9\ 14.9]$ s $\boldsymbol{a_4} = [4.94 \cdot 10^{-7}\ 9.55 \cdot 10^{-6}\ 3.39 \cdot 10^{-6}]$ $\boldsymbol{b_4} = [1.96 \cdot 10^{-6}\ 9.10 \cdot 10^{-6}\ 2.93 \cdot 10^{-6}]$ $\boldsymbol{c_4} = [4.21 \cdot 10^{-7}\ 9.99 \cdot 10^{-6}\ 1.63 \cdot 10^{-6}]$	5235.2

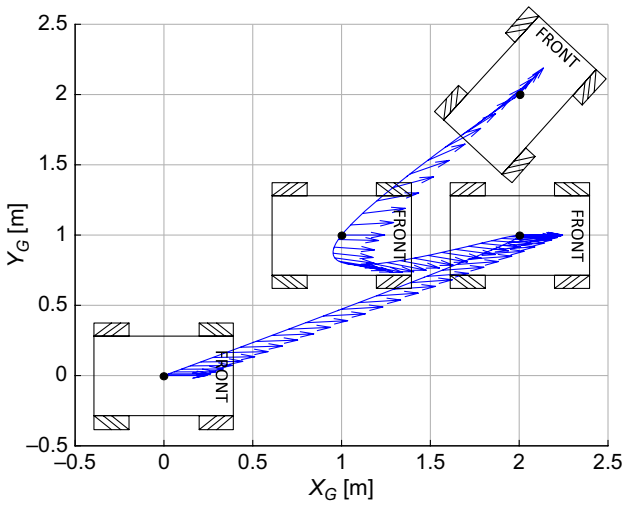

Fig. 9. The energy-optimal trajectories in Simulation 4.

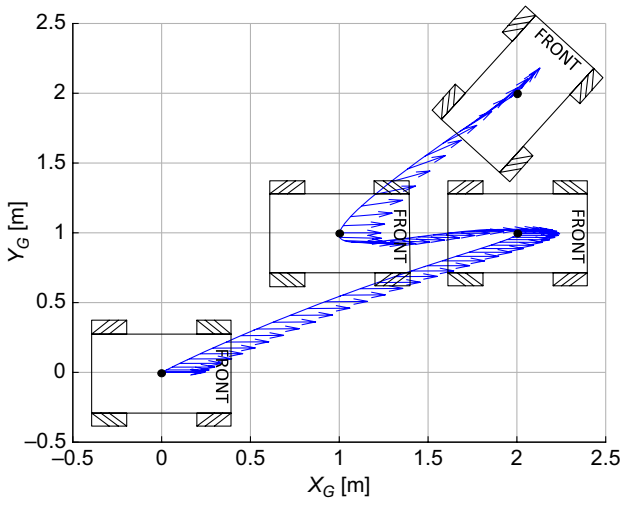

Fig. 10. The energy-optimal trajectories in Simulation 5.

decision variables were $\Delta \boldsymbol{t} = [31.2\ 21.5\ 13.8]$ s, and the resultant optimal energy consumption was 5497.7 J. The resultant energy-optimal trajectories are shown in Fig. 9.

The quartic splines were used in Simulation 5 so that both three spline time variables and nine fourth-order term coefficients were the decision variables. The resultant decision variables are given in Table III, and the resultant optimal energy was reduced by 4.8% to 5235.2 J. The resultant energy-optimal trajectories are shown in Fig. 10. The results of Simulations 4 and 5 are also given in Table III.

https://doi.org/10.1017/S026357471900153X Published online by Cambridge University Press

Table IV. Simulation set#3.

	$\alpha = 0^*$	$\alpha = 0.990$	$\alpha = 0.995$	$\alpha = 0.999$
Simulation 6	1092.2 J (6.5 s)	1173.2 J (4.3 s)	1302.1 J (3.4 s)	2048.5 J (1.8 s)
Simulation 7	1058.1 J (6.2 s)	1171.1 J (3.8 s)	1215.7 J (3.5 s)	2405.6 J (1.4 s)
Simulation 8	987.1 J (6.1 s)	1065.6 J (4.7 s)	1168.2 J (3.3 s)	1980.7 J (1.9 s)
Simulation 9	1805.0 J (11.0 s)	1931.7 J (7.3 s)	2136.4 J (5.8 s)	3342.5 J (3.0 s)
Simulation 10	1788.9 J (10.7 s)	1911.2 J (7.4 s)	2136.2 J (5.8 s)	3440.6 J (3.0 s)

*Energy optimization

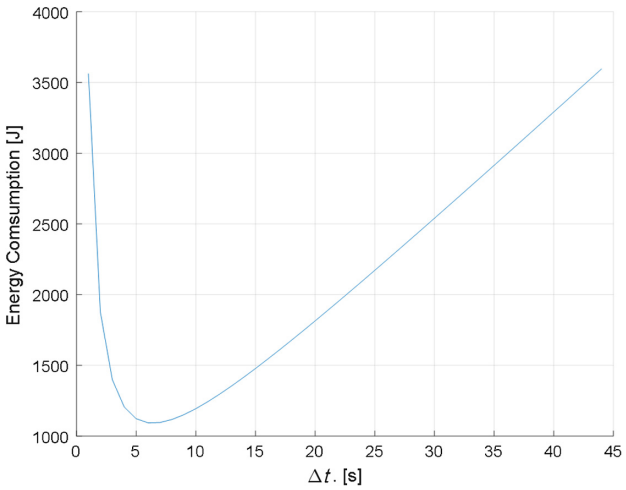

Fig. 11. Energy consumption versus decision variable Δt in Simulation 6.

4.1.3. The third set of five simulations. In this set of simulations, Simulations 6–10, the objective function, F_o, was the task duration $t_n = \sum \Delta t$ and the energy consumption $E\,(T\,(\kappa))$,

$$min_{\kappa}\, F_o\,(\kappa),\;\; F_o = \alpha \cdot t_n \; + (1-\alpha) \cdot E\,(T\,(\kappa)) \tag{26}$$

The weight α varies between 0 and 1. It should be emphasized that the maximum velocity and acceleration constraints of the robot were not included in this set of simulations. A small α did not result in any obvious difference, and α was chosen close to 1 because t_n was a much smaller number than $E(T(\kappa))$. The optimal energy consumption in Simulations 6–10 is given in Table IV.

There was only one single decision variable Δt in Simulation 6 as in Simulation 1. A figure of the energy consumption versus Δt is plotted in Fig. 11.

4.2. Experiments

In the experiments, the resultant energy-optimal velocity trajectories in Simulations 2–4 were executed by the Mecanum robot. Two purposes were for the experiments. The first was to experimentally validate the energy consumption model, by comparing the current and energy consumptions via the model to the actual energy the robot consumes in the experiments. The second was to demonstrate that the robot consumes the minimum energy, by executing the energy-optimal trajectories offline generated.

Based on the optimal decision variables in the simulations, the generated velocity trajectories $\dot{X}(t)$, $\dot{Y}(t)$, and $\dot{\emptyset}(t)$ were set as the desired velocities. Two laser scanners were utilized to measure real-time velocities of the robot in the experiments, and a closed-loop Proportional-Integral (PI) velocity controller was tuned to track the desired velocity trajectories. The current sensors recorded the actual current in the robot's battery that was utilized to calculate the actual energy consumption.

To compare with the desired velocity trajectories, the actual velocity trajectories are shown in Figs. 12 (b), (c), and 13 (a). The actual velocity is marked in black asterisks. There was an initial 2-s delay before the robot started tracking the desired velocity trajectories due to a system delay. The actual position trajectories are shown in Fig. 14, to compare with the desired position trajectories.

https://doi.org/10.1017/S026357471900153X Published online by Cambridge University Press

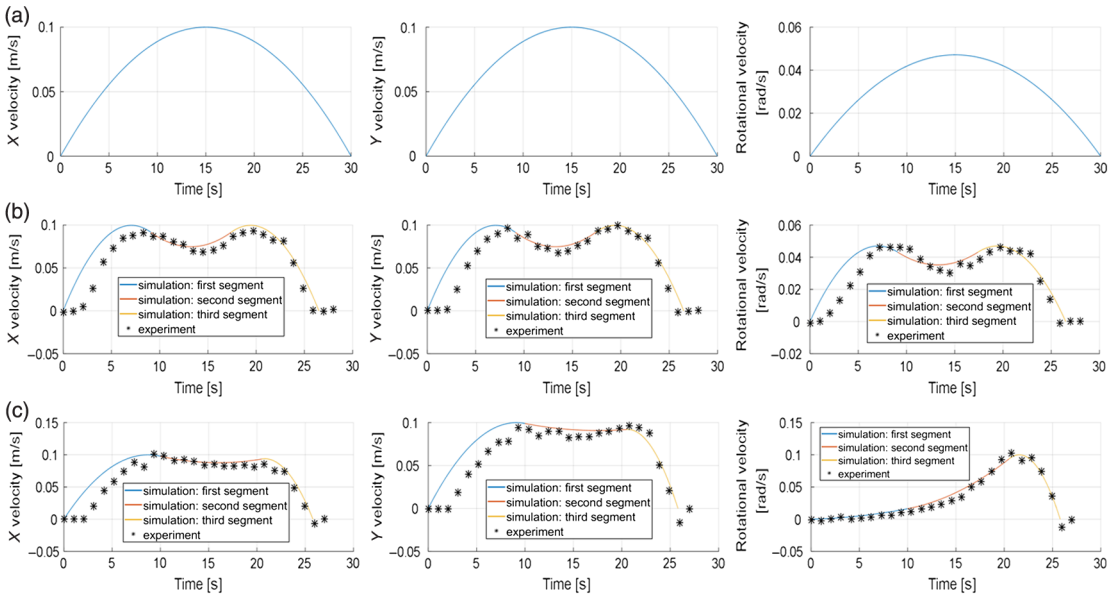

Fig. 12. The velocity trajectories. (a) Simulation 1. (b) Simulation/experiment 2. (c) Simulation/experiment 3.

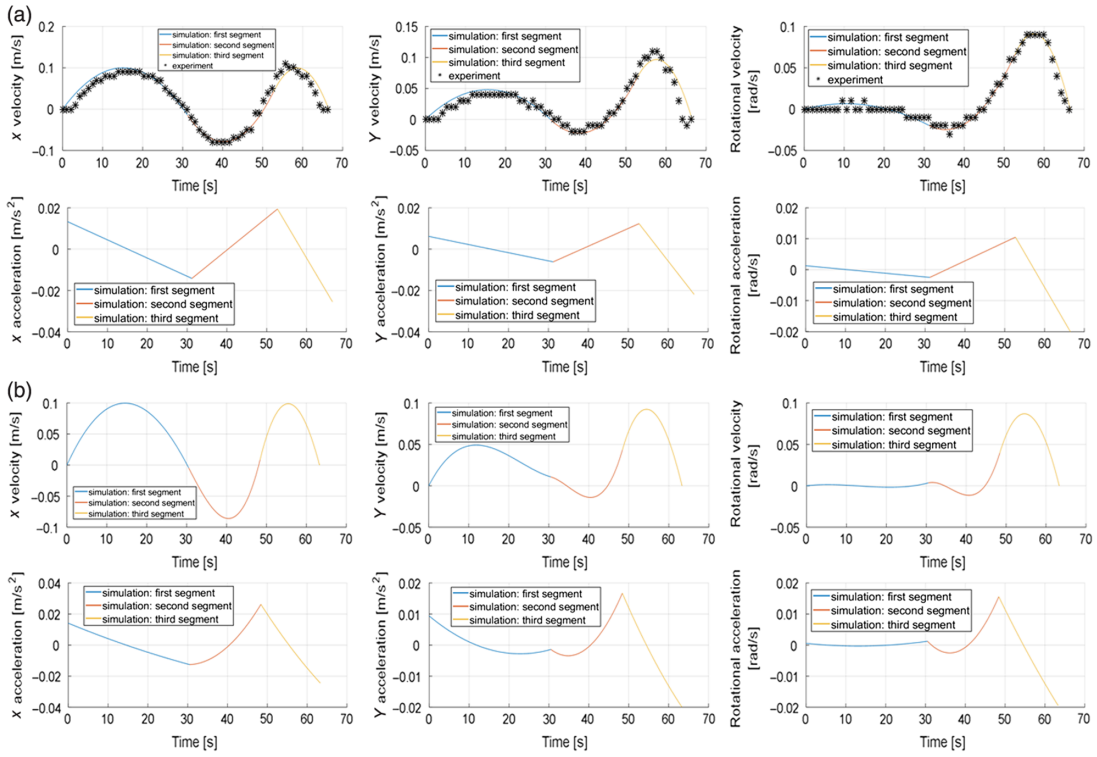

Fig. 13. The velocity and acceleration trajectories. (a) Simulation/experiment 4. (b) Simulation 5.

The actual positions of the robot are drawn in red lines, and the actual orientations are indicated in green arrows. Fig. 14 (a) and (b) shows that the actual position trajectories matched with the desired position trajectories, and Fig. 14 (c) shows that the robot tracked the desired position trajectories within an acceptable tolerance. In order to validate the energy consumption model, the actual and simulated battery current consumptions are plotted in Fig. 15. As the battery provided a stable voltage of 48 V, the actual energy consumption was calculated as 2275.9, 2216.4, and 5466.8 J based on the actual current consumption in Fig. 15 (a), (b) and (c), respectively.

https://doi.org/10.1017/S026357471900153X Published online by Cambridge University Press

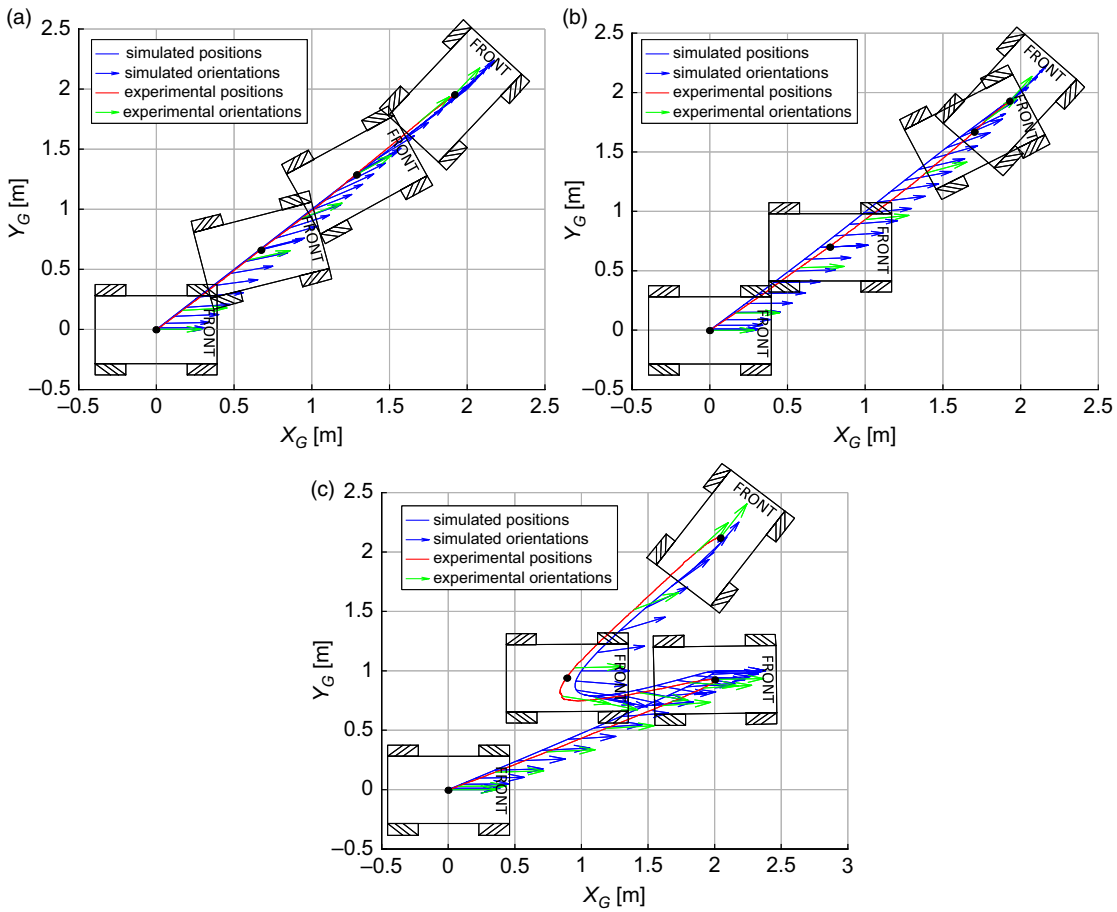

Fig. 14. Desired and actual position trajectories. (a) Simulation/Experiment 2. (b) Simulation/Experiment 3. (c) Simulation/Experiment 4.

4.3. Discussion

The results of Simulations 1–3 in Table II show that increasing the polynomial spline number between the given path points reduces the resultant energy consumption. Comparing with Simulation 1, more polynomial splines were used in Simulations 2 and 3 and consequently less energy consumption was achieved in Simulations 2 and 3 by reducing the task duration. As shown in Fig. 12, the velocity trajectories in Simulation 1 and Simulations 2 and 3 are one segment and three segments of second-order polynomials, respectively. Thus, the task duration can be reduced without increasing the maximum robotic velocities. In addition, the via points were relaxed in Simulation 3 and slightly less energy consumption was achieved in Simulation 3 than in Simulation 2 by avoiding inefficient trajectories, which in this case was translating while rotating, as shown in Fig. 7. The inefficient trajectories were avoided by simultaneously optimizing the via points for path and the polynomial coefficients for trajectory. It is worth mentioning that when the via points in Simulation 3 were taken as the decision variables, additional constraints are included in the optimization problem, which are the variable bounds to the via points as the decision variables as given in Eq. (23). In Simulation 2, the via points were fixed. In Simulation 3, the via points were found by the optimization. Even though in Simulation 3 the relaxed via points were found by the optimization within the variable bounds as the additional constraints, it is still better than fixing the via points as in Simulation 2.

First, according to the results of Simulations 4 and 5 in Table III, higher spline order reduced the resultant energy consumption. A second-order polynomial was used in Simulation 5 to control each segment of acceleration trajectories, while a first-order polynomial was used in Simulation 4, as shown in Fig. 13. Additional decision variables from the higher-order term coefficients in Simulation 5 enable manipulating the acceleration trajectories for better energy optimization. Second, the via points in Simulations 4 and 5 can also be relaxed as additional decision variables. Simulation 4 with

https://doi.org/10.1017/S026357471900153X Published online by Cambridge University Press

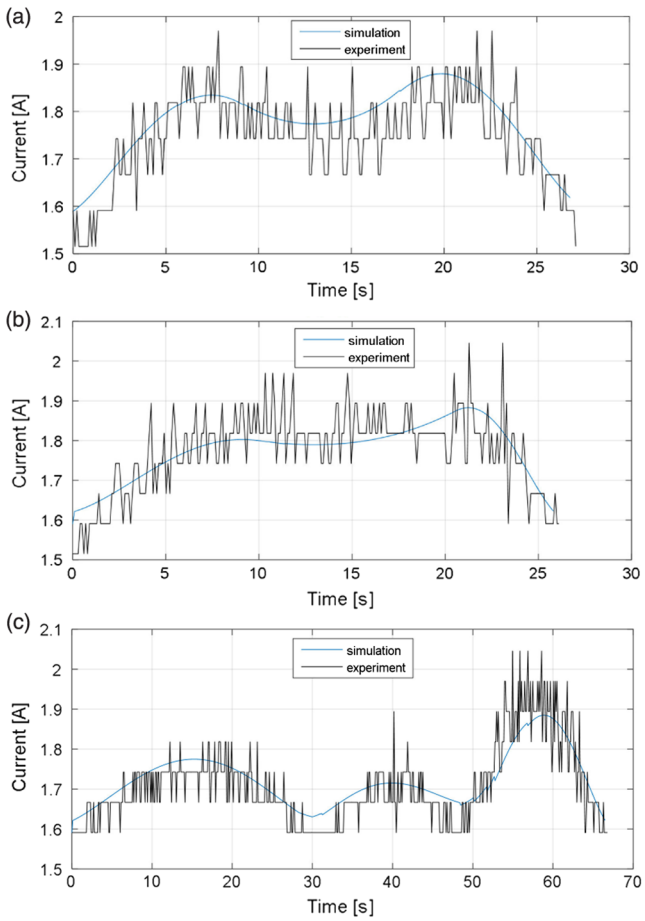

Fig. 15. Battery current plots. (a) Simulation/Experiment 2. (b) Simulation/Experiment 3. (c) Simulation/Experiment 4.

its results would be the same as Simulation 3, if both via points in Simulation 4 were chosen as additional decision variables with the same bounds. Simulation 5 utilized the quartic splines and if the via points were relaxed as additional decision variables, the amount of consumed energy would decrease more, as evidenced by the comparison of the results in Simulations 4 and 5.

The results of Simulations 6–10 in Table IV proved that the minimization of the robotic energy consumption was achieved by only energy consumption as the objective function. The energy consumption of Simulation 6 versus its only decision variable Δt was plotted in Fig. 11. Without the maximum velocity and acceleration constraints of the robot, the minimum-energy consumption was about 1090 J at $\Delta t = 6.5$ s. This was close to the result of Simulation 6 in Table IV. When Δt was smaller than 6.5 s, the energy consumption increased dramatically because the power consumption of faster robotic motion was much higher. When Δt was larger than 6.5 s, the energy consumption increased steadily due to longer task duration.

Furthermore, the energy-optimal motion trajectories were implemented on the Mecanum robot. In the experiments, the robot tracked the generated velocity trajectories that were optimized in simulations. The actual position trajectories matched with the desired position trajectories within an acceptable tolerance. As shown in Fig. 15, the simulated current and energy consumption by the energy consumption model matched with the actual ones measured in the robot. Thus, the energy consumption model was experimentally validated and can further be utilized as the objective function for energy optimization. The actual energy the robot consumed was 2275.9, 2216.4, and 5466.8 J for Simulations 2–4, respectively, which are close to the resultant optimal energy consumption in Tables II and III. So, the robot did consume the minimum energy by tracking the offline-generated energy-optimal trajectories.

https://doi.org/10.1017/S026357471900153X Published online by Cambridge University Press

5. Conclusions

This paper solved a practical issue with industrial Mecanum-wheeled robots in terms of the energy-optimal trajectory generation. The omni-directional motion trajectories of the robot were expressed in polynomial functions that were optimized to fit to a set of path points with the objective function being the energy consumption by the robot. The decision variables for the optimization were the coefficients of the polynomials, the via points, or their combination. A large number of simulations and experiments were conducted, which showed a varying amount of reduction in energy consumption, depending on the chosen set of decision variables.

Acknowledgements

The author L. Xie would like to thank the University of Auckland for awarding the Doctoral Scholarship to him.

References

1. R. Bischoff, U. Huggenberger and E. Prassler, "KUKA youBot—A Mobile Manipulator for Research and Education," *IEEE International Conference on Robotics and Automation (ICRA)*, Shanghai, China (IEEE, 2011) pp. 1–4.
2. F. Adascalitei and I. Doroftei, "Practical Applications for Mobile Robots based on Mecanum Wheels – a Systematic Survey," *Proceedings of International Conference on Innovations, Recent Trends and Challenges in Mechatronics, Mechanical Engineering and New High-Tech Products Development – MECAHITECH'11*, Bucharest, Romania, vol. 3, (2011) pp. 112–123.
3. O. Diegel, A. Badve, G. Bright, J. Potgieter and S. Tlale, "Improved Mecanum Wheel Design for Omni-Directional Robots," *Proceedings of Australasian Conference on Robotics and Automation,* Auckland, New Zealand (2002) pp. 117–121.
4. Y. Mei, Y. H. Lu, Y. C. Hu and C. G. Lee, "Energy-Efficient Motion Planning for Mobile Robots," *IEEE International Conference on Robotics and Automation, Proceedings*, New Orleans, LA, USA, vol. 5 (IEEE, 2004) pp. 4344–4349.
5. Z. Sun and J. H. Reif, "On finding energy-minimizing paths on terrains," *IEEE Trans. Rob*. **21**(1), 102–114 (2005).
6. S. Liu and D. Sun, "Minimizing energy consumption of wheeled mobile robots via optimal motion planning," *IEEE/ASME Trans. Mechatron.* **19**(2), 401–411 (2014).
7. J. Yang, Z. Qu, J. Wang and K. Conrad, "Comparison of optimal solutions to real-time path planning for a mobile vehicle," *IEEE Trans. Syst. Man Cybern. Part A Syst. Humans* **40**(4), 721–731 (2010).
8. I. Duleba and J. Z. Sasiadek, "Nonholonomic motion planning based on Newton algorithm with energy optimization," *IEEE Trans. Control Syst. Technol.* **11**(3), 355–363 (2003).
9. C. H. Kim and B. K. Kim, "Minimum-energy translational trajectory generation for differential-driven wheeled mobile robots," *J. Intell. Rob. Syst.* **49**(4), 367–383 (2007).
10. H. Kim and B. K. Kim, "Online minimum-energy trajectory planning and control on a straight-line path for three-wheeled omnidirectional mobile robots," *IEEE Trans. Ind. Electron.* **61**(9), 4771–4779 (2014).
11. R. P. Paul and H. Zhang, "Robot Motion Trajectory Specification and Generation," *2nd International Symposium on Robotics Research*, Kyoto, Japan (1984).
12. E. Shintaku, "Minimum energy trajectory for an underwater manipulator and its simple planning method by using a genetic algorithm," *Adv. Rob.* **13**(2), 115–138 (1998).
13. L. Tian and C. Collins, "An effective robot trajectory planning method using a genetic algorithm," *Mechatronics* **14**(5), 455–470 (2004).
14. L. Yang, Z. Luo, Z. Tang and W. Lv, "Path Planning Algorithm for Mobile Robot Obstacle Avoidance Adopting Bezier Curve Based on Genetic Algorithm," *Control and Decision Conference (CCDC)* (2008) pp. 3286–3289.
15. L. Xie, C. Henkel, K. Stol and W. Xu, "Power-minimization and energy-reduction autonomous navigation of an omnidirectional Mecanum robot via the dynamic window method local trajectory planning," *Int. J. Adv. Rob. Syst.* **15**(1), 1729881418754563 (2018).
16. L. Xie, W. Herberger, W. Xu and K. A. Stol, "Experimental Validation of Energy Consumption Model for the Four-Wheeled Omnidirectional Mecanum Robots for Energy-Optimal Motion Control," *IEEE 14th International Workshop on Advanced Motion Control (AMC)*, Auckland, New Zealand (IEEE, 2016) pp. 565–572.